CHAPTER 11

Other Magnetic Sensors

Besides the Hall effect and magnetoresistive sensors of the preceding chapter, many other types of magnetic sensors are commonly used. This chapter examines the major remaining types of magnetic sensors.

11.1 SPEED SENSORS BASED ON FARADAY'S LAW

The preceding chapter discussed how a toothed steel wheel rotating next to a Hall sensor is used in many automotive safety systems. In many cases, the speed or velocity is to be sensed, not the position, and thus a pickup coil can be used instead of the Hall sensor, as shown in Figure 11.1. Note that, as in Figure 10.3, a permanent magnet serves as the usual source of the magnetic field. The Hall sensor of Figure 10.3 is replaced in Figure 11.1 by a coil wound around a steel pole piece. A photograph of an actual automotive variable reluctance velocity sensor is shown in Figure 11.2. The cutaway in Figure 11.2 shows the coil, which is wound of hundreds of turns of very thin copper wire.

The voltage induced in the coil is determined by Faraday's law of Equation (2.33):

$$V = -N\frac{d\varphi}{dt} \tag{11.1}$$

where N is the number of turns and φ is the flux passing through the coil. As the toothed steel wheel in Figure 11.1 rotates with angular position θ, the reluctance changes as analyzed in Example 3.2, producing a changing flux through the coil. Assume for simplicity that the flux φ is sinusoidal:

$$\varphi(\theta) = \varphi_{\text{pk}} \sin n_T\theta \tag{11.2}$$

where n_T is the number of teeth on the wheel. Assume that the toothed wheel is rotating at constant mechanical angular velocity Ω in radians per second. Thus:

$$\theta = \Omega t \tag{11.3}$$

Magnetic Actuators and Sensors, Second Edition. John R. Brauer.

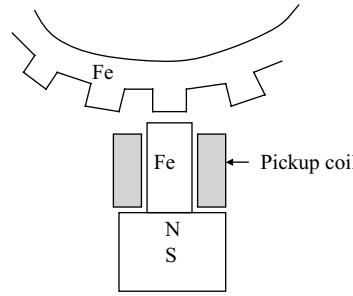

FIGURE 11.1 Toothed wheel speed sensors.

Substituting (11.2) and (11.3) into (11.1) gives:

$$V = -\Omega N n_T \varphi_{\text{pk}} \cos(n_T \Omega t) \tag{11.4}$$

Notice that the magnitude of the induced voltage is proportional to the speed. At very low speed, the voltage is very small. Thus the sensors of Figures 11.1 and 11.2 are indeed speed sensors. While it is true that their voltages can be integrated over time to obtain position, they are inherently speed sensors, not position sensors. In most cases, the coil is open-circuited so that the voltage observed is that of (11.4).

Example 11.1 Speed Sensor Output for Toothed Wheel of Example 3.2 Example 3.2 is to be used as a speed sensor by winding an open-circuited pickup coil of N turns on top of the exciting coil in Figure E3.2.1. Assume that the magnetic flux varies sinusoidally between the values of Example 3.2 and that its armature has n_T teeth equally spaced around 360°. Find the expression for the output voltage as a function of the armature speed Ω.

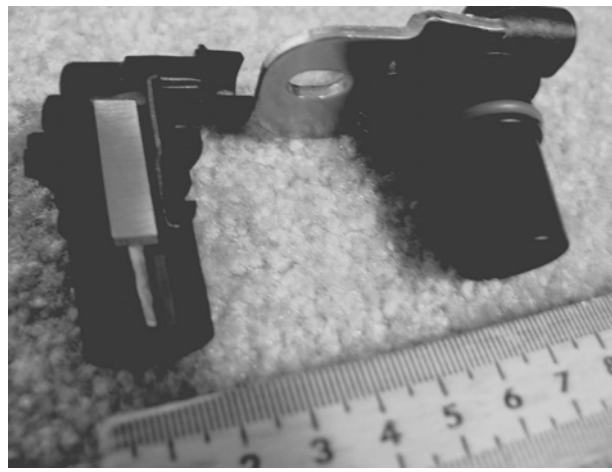

FIGURE 11.2 Actual automotive speed sensor stators, consisting of a coil wound around steel adjacent to a permanent magnet. A cutaway stator is shown to the left of a complete stator.

Solution From Example 3.2, the flux varies from 62.85E−6 to 628.5E−6 Wb. Assuming a sinusoidal variation gives:

$$\varphi(\theta) = 62.85\text{E–}6 + (628.5 - 62.85)\text{E–}6 \sin n_T\theta \qquad \text{(E11.1.1)}$$

Substituting in (11.2) and (11.4) gives the output voltage:

$$V = -\Omega N n_T (566\text{E–}6) \cos(n_T \Omega t) \qquad \text{(E11.1.2)}$$

11.2 INDUCTIVE RECORDING HEADS

The preceding chapter examined magnetoresistive heads for reading (sensing) magnetized media such as hard disks. Besides magnetoresistive heads, inductive heads are commonly used. Inductive heads have a voltage induced by Faraday's law.

Inductive heads are the most common means of writing on, that is, magnetizing, the disk medium. A typical inductive head is shown in Figure 11.3. Its coil is wound with many turns of very fine wire, and therefore, for a given current, the coil can create a much higher magnetizing field intensity than a magnetoresistive head with its single current-carrying conductor. The ampere-turns in the head coil create magnetic flux lines in the disk medium. Inductive heads can also be used for reading, that is, sensing the magnetic field pattern written on the disk. However, their reading performance is usually inferior to that of magnetoresistive heads.

The inductive head read signal is based on Faraday's law, as is the signal produced by a moving-magnet microphone. For simplicity, assume that a sinusoidal pattern is magnetized on the recording disk and produces the flux of (11.2) linking the head coil:

$$\varphi(\theta) = \varphi_{\text{pk}} \sin n_C\theta \qquad (11.5)$$

where the number of teeth n_T of (11.1) is changed to n_C, the number of cycles of magnetization along the disk track circumference. Assuming the disk is traveling at

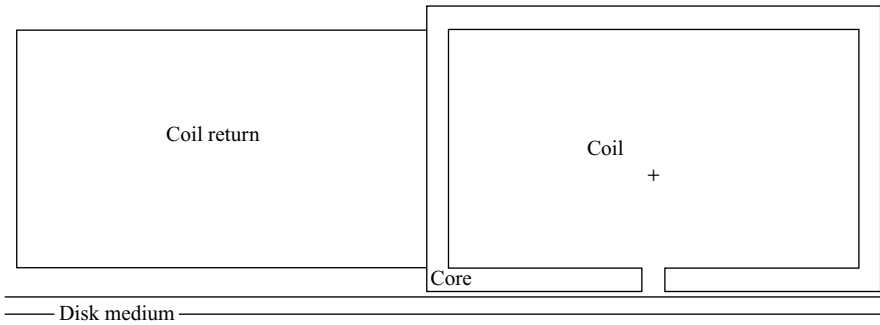

FIGURE 11.3 A typical inductive head and adjacent disk medium.

angular speed Ω in radians per second, then, from Faraday's law, the signal volts "read" at the head coil is similar to (11.3), becoming:

$$V = -\Omega n_C N \varphi_{\text{pk}} \cos(n_C \Omega t) \tag{11.6}$$

Since φ_{pk} is produced by one magnetized bit (half cycle) on the disk, it equals B_{pk} times the area of a half cycle. Thus:

$$\varphi_{\text{pk}} = B_{\text{pk}}(2\pi r_{\text{disk}} w_{\text{track}})/(2n_c) \tag{11.7}$$

where r_{disk} is the disk radius, and w_{track} is the disk magnetization track width. The flux density B_{pk} is limited by saturation, etc. Substituting (11.7) in (11.6) gives:

$$V = -\Omega r_{\text{disk}} \pi w_{\text{track}} N(B_{\text{pk}}) \cos(n_C \Omega t) \tag{11.8}$$

Notice that the magnitude of the voltage sensed is proportional to the product of the angular speed Ω times the disk radius. When the radius is reduced by disk drive miniaturization, the read voltage of (11.8) is reduced. In contrast, the voltage of a magnetoresistive read head is proportional only to the change in flux density, not speed. Thus magnetoresistive read heads have almost totally replaced inductive read heads in hard disk drives.

The magnetization pattern produced on the disk medium in actual operation depends on the history of all previous write operations. Predicting all such hysteresis effects is a very challenging task. Several books and a huge number of technical papers continue to be written about magnetic recording [1,2] and magnetic hysteresis [3,4]. Also, all permanent magnets used in actuators and sensors must undergo magnetization, and modeling their *magnetizing fixtures* requires similar techniques [5].

As mentioned in Chapter 1, disk drives often utilize the read signal of the head as a position sensor for the voice coil actuator in a feedback control servo system [1]. The voice coil actuator must *seek* the desired track in minimum time for rapid information transfer to or from the disk [6, 7].

Example 11.2 Writing and Reading with an Inductive Head The inductive head of Figure E11.2.1 is to be used for both writing and reading. It has 20 turns of wire carrying 0.05 A for writing. Assume that the disk medium has a relative permeability of 3 and has been previously unmagnetized. Dimensions of the head core, of relative permeability 2000, are 80 μm in x and 50 μm in y. The head core is 4 mm deep in the z direction. The medium is 3 mm thick in the radial direction and spaced by 1 mm from the head.

(a) Find the field in the disk medium during writing using Maxwell. Assume all eddy currents are negligibly small.

(b) If the coil current is reset to zero, and the section of the disk between the head poles (below the head airgap) is magnetized with $B_r = 0.5$ T in the direction parallel to the disk, find the flux pattern throughout the medium and head.

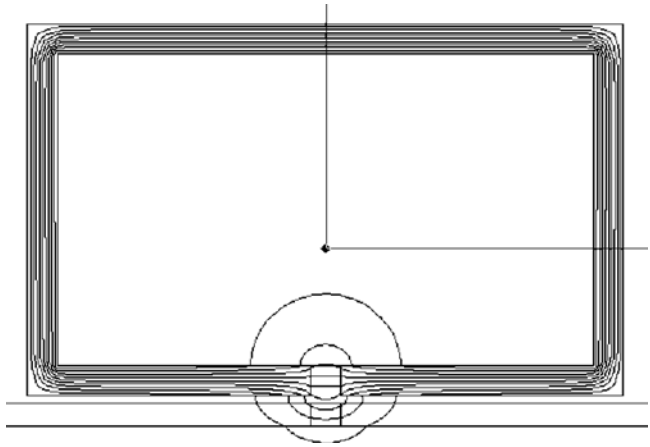

FIGURE E11.2.1 Computer display of an inductive head with computed flux lines during write operation on a previously unmagnetized disk.

Solution Maxwell's magnetostatic solver was first used with no permanent magnet materials, and later with the bit region being permanently magnetized with $B_r = 0.5$ T in the direction parallel to the disk.

(a) Computed flux lines are shown in Figure E11.2.1. All flux densities are less than 2 T, with the highest densities in the head core.

(b) The computed flux lines are shown in Figure E11.2.2. All flux densities are less than 0.3 T, with the highest density in the bit. Most of the head core has flux density on the order of 0.15 T, less than 10% of its flux density during writing.

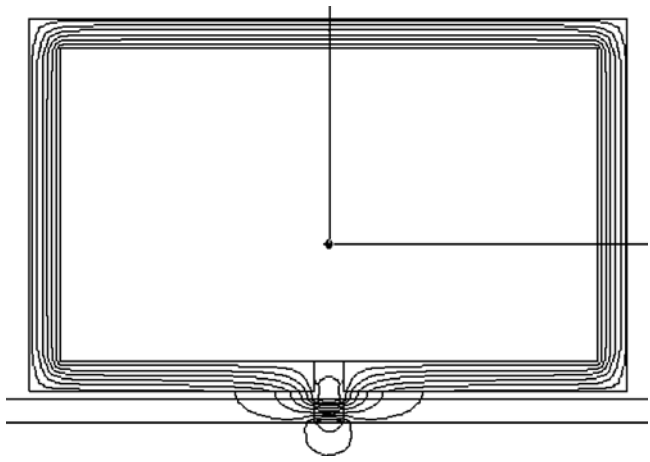

FIGURE E11.2.2 Computer display of an inductive head with computed flux lines produced by a single bit on the disk immediately below the head gap.

11.3 PROXIMITY SENSORS USING IMPEDANCE

The AC impedance seen by a coil depends on its surroundings. If the adjacent surrounding vicinity, called the proximity, contains conducting and/or permeable objects, then the impedance can be significantly changed. Thus coils carrying AC currents are often used as *proximity sensors.*

Since metal objects are always conducting, proximity sensors are commonly used to detect their presence nearby. For example, metal detectors for security systems commonly include proximity sensors. The impedance they see, that is, their ratio of complex AC voltage to complex AC current, is affected by the eddy currents induced in the metal. Thus proximity sensors are also commonly called *eddy current sensors.*

Besides security systems, proximity eddy current sensors are also commonly used in factory automation. For example, such sensors are used to determine when a metal part is approaching a station on an assembly line, so that a robot can find and work on the part. In both security and automation applications, the sensor output signal must undergo either simple or advanced signal processing to determine the next action.

The object being sensed is often called the *target*. Most eddy current proximity sensors detect the target using frequencies of 50 Hz through about 100 kHz. Both real and imaginary parts of the sensor impedance are usually monitored in order to detect the target and its location.

11.3.1 Stationary Eddy Current Sensors

The first step in understanding proximity sensors is to analyze such sensors when the target is not moving, or moving so slowly that motional eddy current effects are negligible. The effects of higher speed motion will be investigated later.

An example of a proximity sensor is shown in Figure 11.4. It is basically a solenoid actuator with a clapper armature that is the target. The sense coil is wound on a steel stator core that is preferably laminated. The sensor of Figure 11.4 was analyzed by two-dimensional planar AC finite-element analysis.

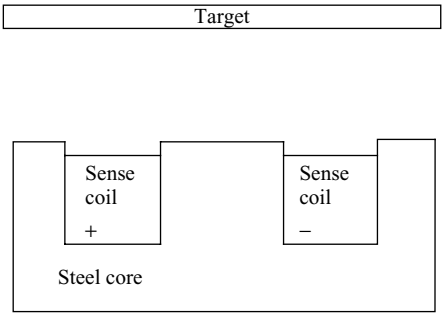

FIGURE 11.4 A typical proximity sensor.

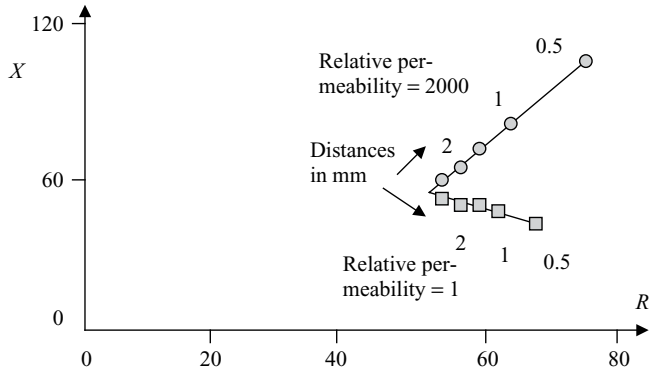

FIGURE 11.5 Impedance plane plots for proximity sensor of Figure 11.4 with various targets and positions. The target has conductivity 1.E7 S/m and a relative permeability of either 2000 or 1. The frequency is 1 kHz. The airgap distance between the stator poles and the target is 0.5 mm or greater.

The plot of complex-plane impedance for two target materials and multiple positions is shown in Figure 11.5 for frequency of 1 kHz. Ideally, the frequency should be selected to see the greatest impedance changes with variable target materials and positions. Note that the higher permeability target material gives higher inductive reactance X than the lower permeability material, as one would expect. Note also that the resistive R (lossy) component in Figure 11.5 rises as the target approaches, due to the conductive losses in the target. The target material and its distance can thus be determined from the complex-plane impedance.

Note in Figure 11.5 that as the target approaches, the impedance follows a path called a locus. The complex-plane impedance locus is thus very revealing of the target.

Complex-plane impedance loci are commonly used in *non-destructive testing (NDT) and non-destructive evaluation (NDE).* For example, an AC current-carrying coil can be moved along a steel pipe. Any changes in the eddy current flow patterns of the pipe due to cracks, imperfect geometries, etc. will cause changes in the impedance locus. Many books and papers are devoted to electromagnetic sensors for NDT and NDE [8, 9].

In NDE, the evaluation of the complex-plane impedance locus is a type of *inverse problem.* Signal processing software is employed to attempt to determine the type of any flaw and its severity. Examples include pipes in nuclear power plants and security checkpoints at airports. Certain NDE signals are caused by unacceptable metallic flaws that must be detected in order to register an alarm. Another example is eddy current sensors suspended down holes in the earth; their signals are determined by subterranean conductivities and can thus be processed to find petroleum.

Any sensor must, to some extent, perturb the object being sensed. Eddy current proximity sensors produce forces on their metallic targets. For example, the sensor of Figure 11.4 is also a magnetic solenoid actuator with the target as the armature. The

armature forces of Chapters 7 and 8 act on the target. Whereas the actuator designer usually seeks to maximize the force and resultant armature motion, in most cases, the sensor designer seeks to minimize the target force and motion. Because eddy current prediction by hand calculation is extremely difficult, usually electromagnetic finite-element analysis is carried out instead.

Example 11.3 Impedance of Proximity Sensor for Two Target Positions An eddy current proximity sensor of the type of Figure 11.4 is to be used with an aluminum target. The stator is identical to the steel stator of Example 7.1, but it is now laminated. The stator coil consists of 10 turns, each carrying 0.2-A rms. The armature material is now aluminum of conductivity 3.6E7 S/m. The target and sensor are shown in Figure E11.3.1. The coil resistance is 0.1 mΩ. The impedance seen by the coil is to be found for airgap distances of 2 mm and 4 mm using Maxwell.

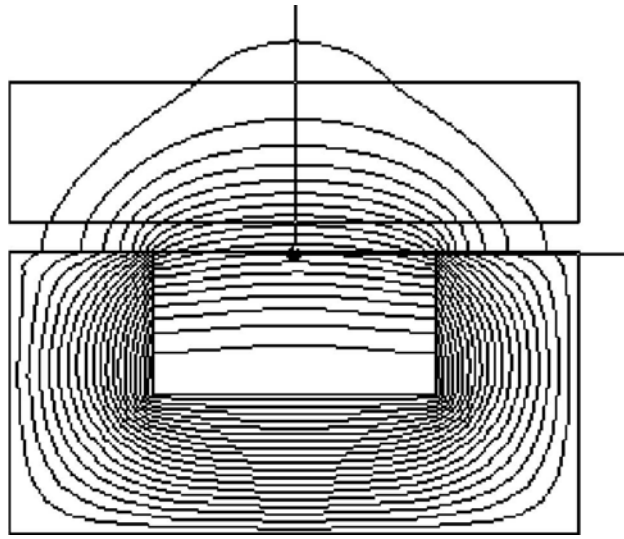

FIGURE E11.3.1 Computer display of a proximity sensor and its computed flux lines.

Solution The easiest way to make this model is to begin with the model of Example 7.1. Changes required include making the solution type "Eddy Current" and changing the armature material. For the original 2-mm airgap, the flux linkage output for 1 turn is $\lambda = 2.375\text{E}{-6} - j1.195\text{E}{-7}$. The series impedance for one turn is then found using (6.30):

$$Z = j\omega\lambda / I \tag{E11.3.1}$$

where $I = 2$ A and $\omega = 377$. The resulting series impedance (for 10 turns) is:

$$Z_s = R_s + jX_s = (10)(22.53\text{E}{-6} + j448.\text{E}{-6}) = 22.53\text{E}{-5} + j448\text{E}{-5} \tag{E11.3.2}$$

The total impedance is found by adding the 0.1-mΩ coil resistance (as explained in Chapter 8), obtaining:

$$Z(0.002) = 32.53\text{E}{-5} + j448\text{E}{-5} \tag{E11.3.3}$$

The corresponding flux lines are shown in Figure E11.3.1.

To obtain results at the 4-mm position, the armature is moved upward by 2 mm using the "Arrange" and "Move" commands. The flux linkage output for 1 turn is $\lambda = 2.66\text{E}{-6} - j8.215\text{E}{-7}$, greater evidently because the aluminum is further away and repels less flux. The series impedance for one turn is then found using (6.30):

$$Z = j\omega\lambda/I \tag{E11.3.4}$$

where $I = 2$ A and $\omega = 377$. The resulting series impedance (for 10 turns) is:

$$Z_s = R_s + jX_s = (10)(155\text{E}{-6} + j501.4\text{E}{-6}) = 155\text{E}{-5} + j501\text{E}{-5} \tag{E11.3.5}$$

The total impedance is found by adding the 0.1-mΩ coil resistance to obtain:

$$Z(0.004) = 165\text{E}{-5} + j501\text{E}{-5} \tag{E11.3.6}$$

11.3.2 Moving Eddy Current Sensors

The effect of target velocity on the sensor signal is indicated by the *magnetic Reynolds number* [10]:

$$R_m = \mu\sigma Vl \tag{11.9}$$

where V is the velocity and l is the length of the conductive armature in the direction of the velocity and motion. The magnetic Reynolds number is dimensionless. If it is less than one, then the velocity effects are negligible, and the methods of the preceding section apply.

If R_m exceeds one, then the velocity effects are significant. The larger R_m, the more the magnetic flux distribution is altered by motional induced voltage. Hence magnetic actuators and sensors with high magnetic Reynolds numbers must be analyzed including velocity effects. Usually magnetic actuators have zero armature speed at time zero, and rarely reach speeds with high Reynolds numbers. However, in the case of *magnetic brakes,* the speed is high and is reduced by eddy current braking forces [11, 12].

Magnetic sensors often sense objects with high velocities and high Reynolds numbers. An example is NDE sensors for steel heat exchanger tubes in nuclear

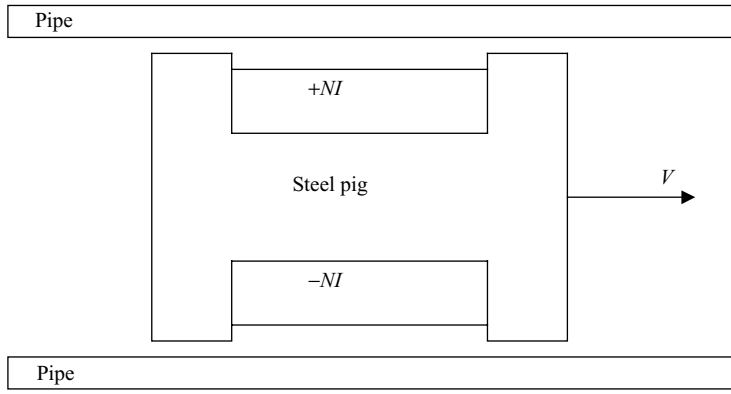

FIGURE 11.6 A typical AC eddy current NDT sensor traveling through a pipe.

power plants or for pipelines made of steel. These eddy current sensors are often pulled through pipes at fairly high velocities, and thus R_m often exceeds one. A typical traveling sensor, often called a pig, is shown in Figure 11.6. Note that if there is no defect in the pipe, then the geometry of Figure 11.6 does not change with time, even though there is a relative velocity between the pig and the pipe. A perfect or *smooth* pipe becomes an imperfect pipe if there is any roughness on its surface due to corrosion cracks, etc.

Finite-element methods have been developed for such problems with smooth conducting armatures traveling at constant high velocities [11, 12]. In such formulations, the matrix equation becomes unsymmetric [12]. For more general moving armatures with imperfect non-smooth (changing) geometry with motion, finite-element methods will be discussed in Chapters 14 and 15.

11.4 LINEAR VARIABLE DIFFERENTIAL TRANSFORMERS

The variation of magnetic sensor signal with position is often nonlinear, whereas a linear correspondence between position and signal voltage is highly desirable. For example, the proximity sensor impedances of Figure 11.5 and of Example 11.3 are not linear with position.

A sensor with an extremely linear relation between position and voltage magnitude is the *LVDT, linear variable differential transformer.* A typical LVDT is shown in Figure 11.7 and is made of E-shaped steel, laminated to make the magnetic Reynolds number nearly equal to zero. The LVDT has a primary winding excited with AC voltage V_p. It also has two secondary windings with induced open-circuit voltages V_{s1} and V_{s2}.

The two secondary voltages are induced by Faraday's law transformer action, and are equal and opposite if the laminated steel armature is at zero position, that is, centered below the primary winding and its laminated steel pole. If the armature is positioned to the right (a positive position x), then the total induced voltage $V_{s2} - V_{s1}$

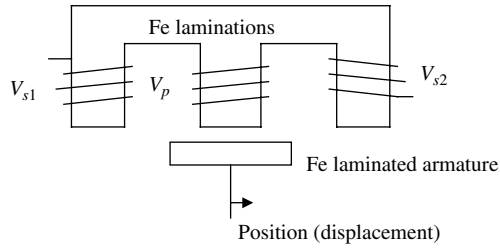

FIGURE 11.7 A typical LVDT.

is positive and proportional to x. The relation between the LVDT voltage output $V_s = V_{s2} - V_{s1}$ and x is shown in Figure 11.8.

Various LVDT designs are possible, and the frequency of operation may also vary. Typical frequencies range from 50 Hz to 25 kHz. Figure 11.8 shows that the output voltage increases with frequency, but can be extremely linear with position. Note also that the voltage is reduced as the load impedance is reduced.

LVDTs are unfortunately quite expensive. Their optimum frequency usually lies from 500 Hz to 5 kHz. To generate this frequency, electronics required includes the following.

- A 60 Hz to DC power supply
- An oscillator of the desired frequency
- A phase shifter
- AC and DC amplifiers

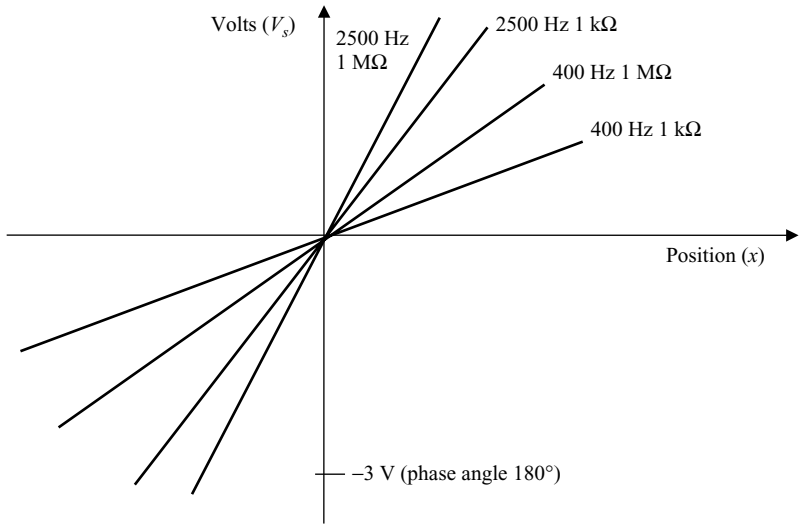

FIGURE 11.8 Typical voltage versus position curves of LVDT.

Example 11.4 Simple LVDT An LVDT is shown in Figure E11.4.1 as drawn in Maxwell's drawing window. The primary coil consists of 1000 turns, each carrying 2-A rms 1000 Hz. Both the stator and armature are made of laminated steel with relative permeability 2000. The two secondary coils indicated by the arrows are open-circuited and connected in series opposition, each having 500 turns. Use Maxwell to find the total secondary output voltage for the 20-mm × 6-mm armature at centered (zero) position and moved 4 mm to the right. The depth into the page is 100 mm.

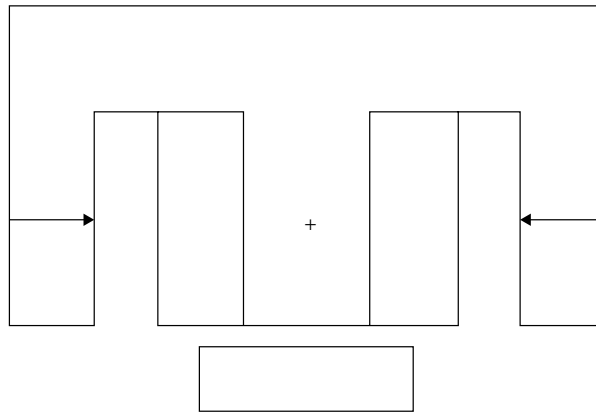

FIGURE E11.4.1 Geometry of LVDT to be modeled.

Solution Since there are no significant eddy currents, a magnetostatic solution suffices. The model shown in Figure E11.4.1 was input into Maxwell to find the flux passing through the two secondary coils. The computed flux plot at zero armature position is shown in Figure E11.4.2. The computed secondary fluxes are −2.93E−5

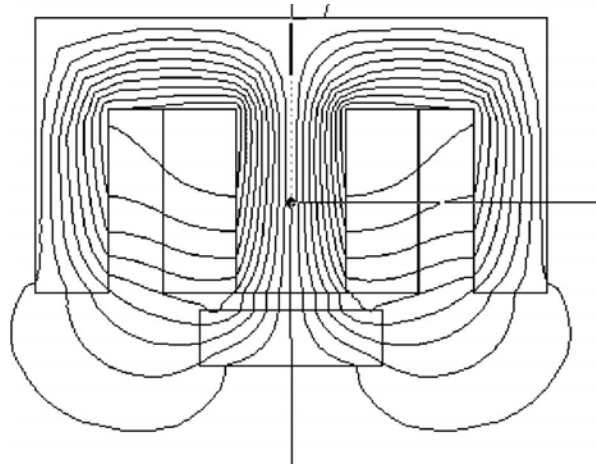

FIGURE E11.4.2 Computer display of flux lines computed in LVDT for armature position = 0.

and +2.94E−5 Wb, the magnitudes differing due solely to the mesh not being perfectly symmetric. The induced voltage is thus approximately zero.

Next, the "Arrange" and "Move" commands were used to move the armature 4 mm to the right. The computed secondary fluxes are −2.59E−5 and +3.58E−5 Wb for 1 m depth. For the actual 0.1 m depth, the total flux linking the secondary is thus +0.99E−6 Wb. To find the secondary voltage magnitude, use Faraday's law:

$$|V| = N\mathrm{d}\phi/\mathrm{d}t = N\omega\phi = 2\pi f N\phi \tag{E11.4.1}$$

Substituting the total flux, frequency, and 500 turns, the LVDT output for this position is 3.11 V.

11.5 MAGNETOSTRICTIVE SENSORS

Magnetostriction is the phenomenon of elastic deformation that accompanies magnetization [13]. Magnetic fields cause certain materials to deform. This deformation is a form of motion in magnetostrictive and *magnetorheological* actuators. However, motions of such actuators are usually much less than 1 mm, and thus magnetostrictive actuators are not further discussed in this book.

Magnetostrictive sensors, on the other hand, are useful and fairly commonplace. They require, however, materials in which magnetic flux density and mechanical properties are strongly interdependent. While steel has small magnetostrictive effects, recently developed materials exhibit much stronger magnetostriction.

The material constitutive properties are determined by the following matrix equation for planar magnetostriction:

$$\begin{bmatrix} \sigma_{xx} \\ \sigma_{yy} \\ H_x \\ H_y \end{bmatrix} = \begin{pmatrix} K_1 & K_2 & X_1 & X_2 \\ K_3 & K_4 & X_3 & X_4 \\ X_5 & X_6 & M_1 & M_2 \\ X_7 & X_8 & M_3 & M_4 \end{pmatrix} \begin{bmatrix} \varepsilon_{xx} \\ \varepsilon_{yy} \\ B_x \\ B_y \end{bmatrix} \tag{11.10}$$

Note that the left-hand column vector contains both planar structural stresses σ and magnetic field intensities. The right-hand column vector contains both planar structural strains ε and magnetic flux densities. The 4×4 matrix is the material tensor, containing purely structural entries K, purely magnetic entries M, and magneto-mechanical coupling cross-term entries X.

A strongly magnetostrictive material is Terfenol-D, which is made up of rare earth elements Tb (terbium), Dy (dysprosium), and also Fe. A typical Terfenol-D actuator is shown in Figure 11.9. Application of a magnetic field causes the Terfenol-D membrane to bend.

A commonly used magnetostrictive position sensor is shown in Figure 11.10. The magnetostrictive material acts as an acoustic waveguide. The linear position sensor is composed of four elements.

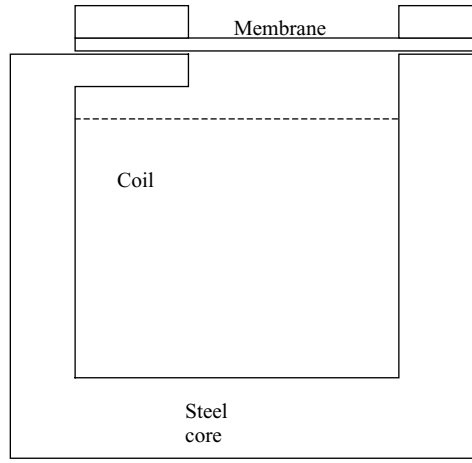

FIGURE 11.9 A magnetostrictive actuator with Terfenol-D membrane.

(1) Waveguide sensing element
(2) Sensing and output conditioning electronics module
(3) Protective housing
(4) External permanent magnet

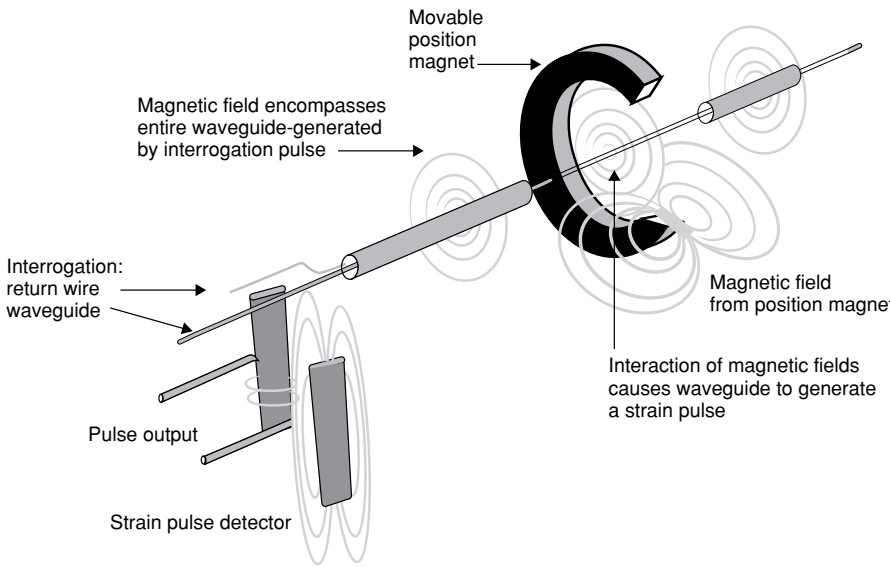

FIGURE 11.10 A magnetostrictive position sensor. This picture of a Temposonics® sensor is courtesy of MTS Sensors.

A sonic strain pulse is induced in the magnetostrictive waveguide by the momentary interaction of two magnetic fields. One field comes from a movable permanent magnet which passes along the outside of the sensor tube, while the other field comes from a current pulse or interrogation pulse applied along the waveguide. The interaction of the two magnetic fields produces a strain pulse, which travels at sonic speed along the waveguide until the pulse is detected at the head of the sensor. The position of the magnet is determined with high precision by measuring the elapsed time between the application of the interrogation pulse and the arrival of the resulting strain pulse. Hence accurate non-contact position sensing is achieved without any wear to the sensing components.

Another popular use of magnetostrictive sensors is for torque sensing. For control of rotating electric motors or internal combustion engines, accurate sensing of shaft torque is often required. Since the shaft is rotating, connecting it directly to electrical sensing wires is highly impractical. Instead, the strain in the shaft can be measured with a non-contact magnetostrictive sensor [14], and the strain is proportional to torque.

11.6 FLUXGATE SENSORS

Materials such as steel with nonlinear B–H curves can be used to make *fluxgate sensors.* The sensor material is driven between the constant-permeability and the saturable regions of its B–H curve. A typical fluxgate sensor is shown in Figure 11.11. The inductance seen by its coil is a function both of its coil current and the external magnetic field to be sensed.

Fluxgate sensors are used as proximity sensors, for navigational and geomagnetic field measurement instruments, compasses, and for position and speed sensing. A

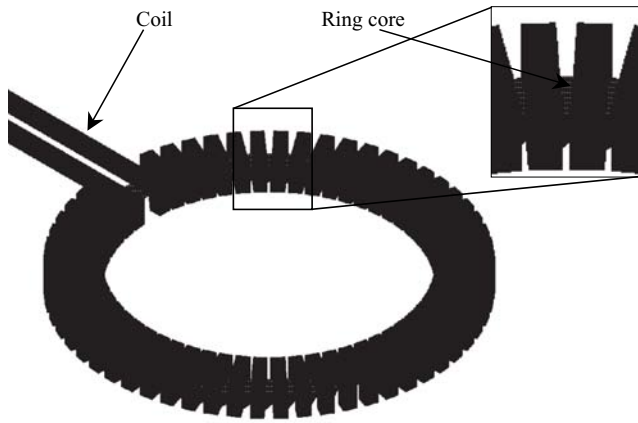

FIGURE 11.11 Computer display of a typical fluxgate sensor with a toroidal coil wound on a ring core.

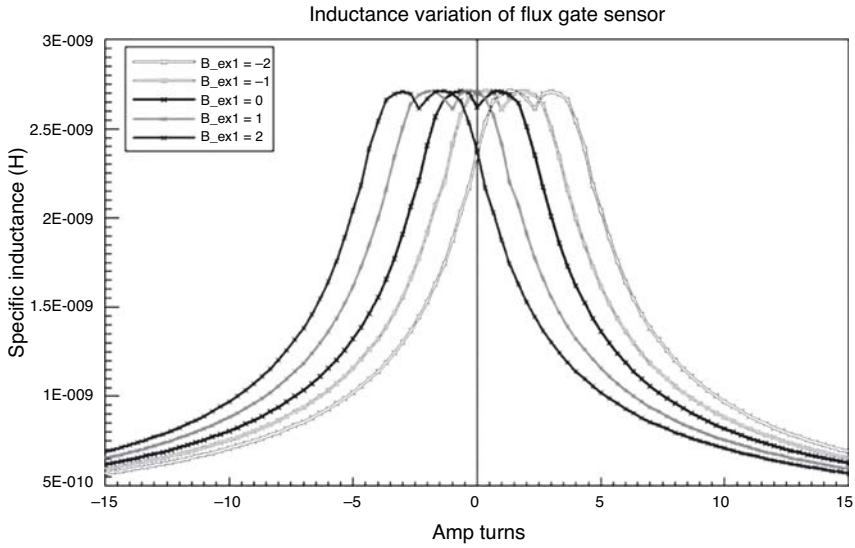

FIGURE 11.12 Typical fluxgate sensor inductance variation.

properly designed fluxgate sensor has an output linearly proportional to the magnetic field being sensed.

Finite-element analysis aids the design of fluxgate sensors [15]. The inductance seen by the coil for various external magnetic flux densities computed for a typical fluxgate sensor is plotted in Figure 11.12. Note how the curves shift with the external field. The curves can then be exported from the Maxwell finite-element software to a circuit analysis program such as SPICE or Simplorer®. SPICE, which stands for Simulation Program with Integrated Circuit Emphasis, is widely available in several forms, as will be discussed in Chapter 15. Simplorer, available from Ansys, Inc., is a software package used to design and analyze complex technical systems.

Typical saturable sensor current response to an applied 2.5-V, 100-kHz sinusoid is shown in Figure 11.13 for no applied external field. When an external field is applied,

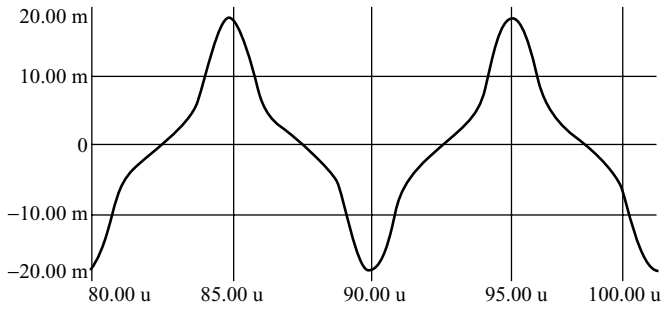

FIGURE 11.13 Typical fluxgate sensor current response to an applied 2.5-V 100-kHz sinusoid with no external magnetic field. Note that the positive and negative areas are equal.

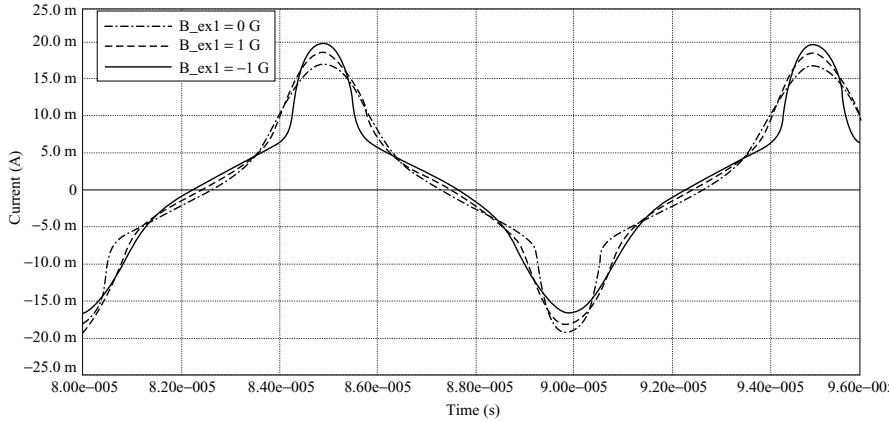

FIGURE 11.14 Typical fluxgate sensor current response to an applied 2.5-V 100-kHz sinusoid with applied external magnetic fields. Note that the positive and negative areas are unequal when an external field is applied.

the current response is shifted as shown in Figure 11.14. The sensor behaves similarly when excited with a square wave voltage, as shown by the current in Figure 11.15. Thus fluxgate sensors are often driven by a square wave voltage such as shown in Figure 11.16. Such a voltage can be created by two alternately fired MOSFETs as shown in Figure 11.17. The sensing circuit Simplorer model, including SPICE models of op-amp integrated circuits, is shown in Figure 11.18. The output voltage of Figure 11.18 is shown in Figure 11.19 for various fields to be sensed [15].

In many cases, there are two external fields to be sensed, and the differential flux density between the two is to be found. The final fluxgate sensor model for such a system is shown in Figure 11.20. The MOSFETs are fired by state machines. The

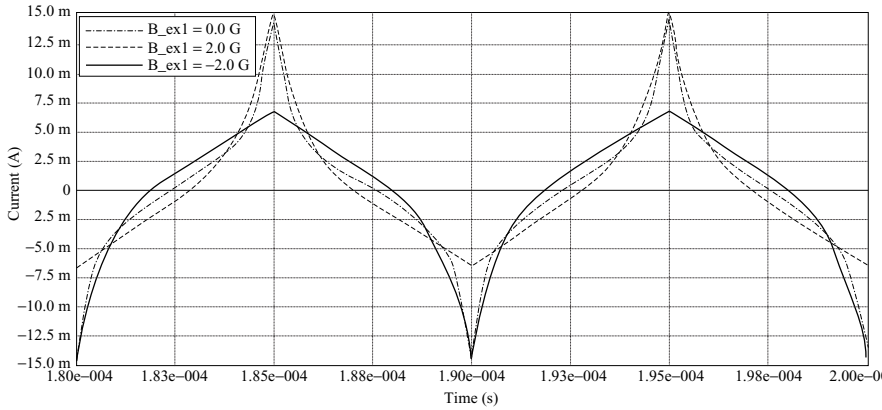

FIGURE 11.15 Typical fluxgate sensor current response to an applied 1.5-V 100-kHz square wave with applied external magnetic fields. Note that the positive and negative areas are unequal when an external field is applied.

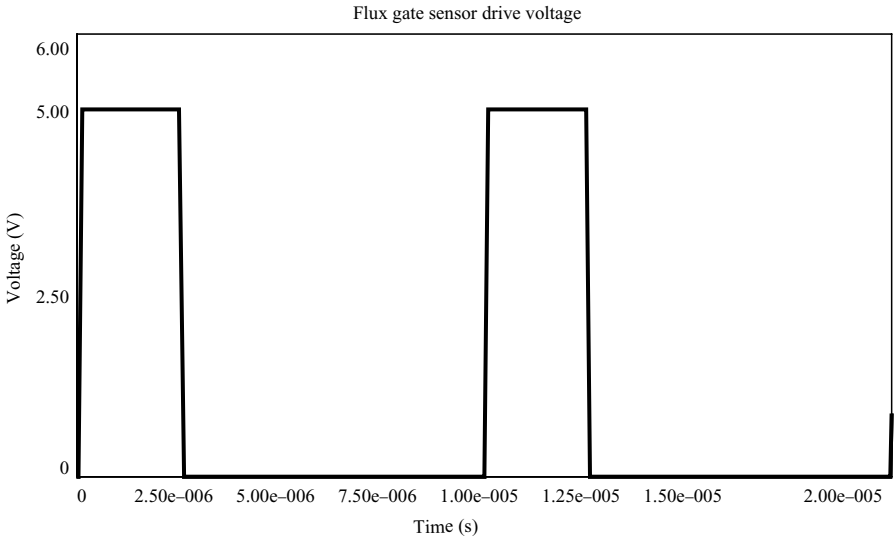

FIGURE 11.16 Typical square wave voltage applied to fluxgate sensor.

system model transient response to a change in the external field from 0 to −0.2 mT is shown in Figure 11.21. Thus the response time of the fluxgate sensor is shown to be in the millisecond range [15]. Fluxgate sensors are able to detect even smaller flux densities, down to the 0.1 nT range.

Somewhat similar to fluxgate sensors in use of nonlinear *B–H* materials is the *Wiegand wire* sensor patented in 1974 [16]. It has an outer coating or shell with high coercive force that surrounds a core of soft magnetic material. At the instant when the outer shell is fully magnetized and the core begins to carry flux, both the core and shell switch magnetization polarity. This flux switch generates a significant voltage. Thus Wiegand wire sensors are often used in place of the Hall sensors in the encoders of Figure 10.4, producing voltage pulses on the order of 1–10 V.

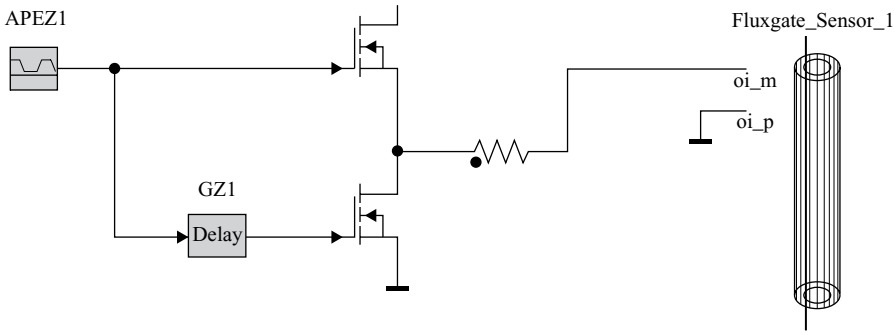

FIGURE 11.17 A typical fluxgate sensor drive circuit containing two MOSFETs, modeled in Simplorer.

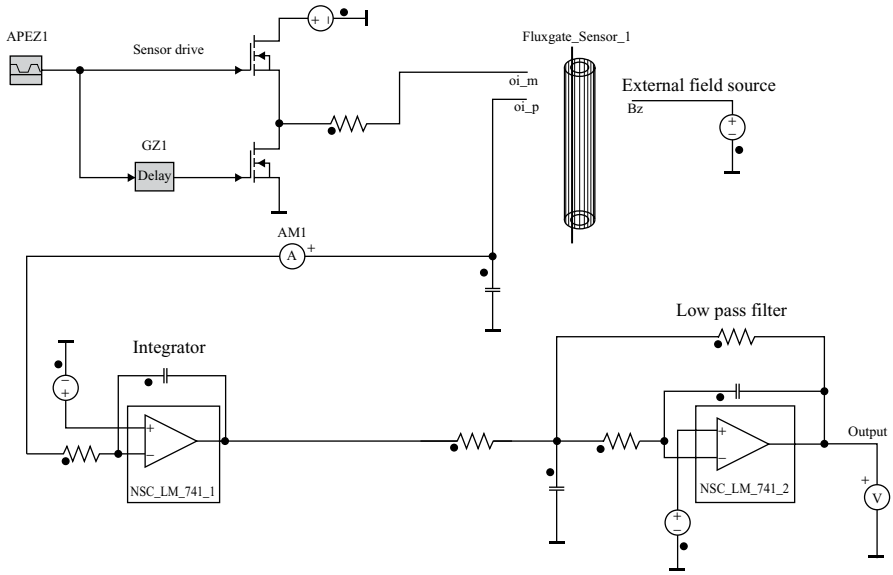

FIGURE 11.18 A typical Simplorer model of fluxgate sensor, including op-amp integrated circuit models originally developed for SPICE.

11.7 CHATTOCK COIL FIELD AND CURRENT SENSOR

A sensor for AC magnetic fields and currents near iron is the *Chattock coil* shown in Figure 11.22. Note that the Chattock coil has a small-diameter winding of long arc length l, which is often semicircular as shown. Because the Chattock coil has an air

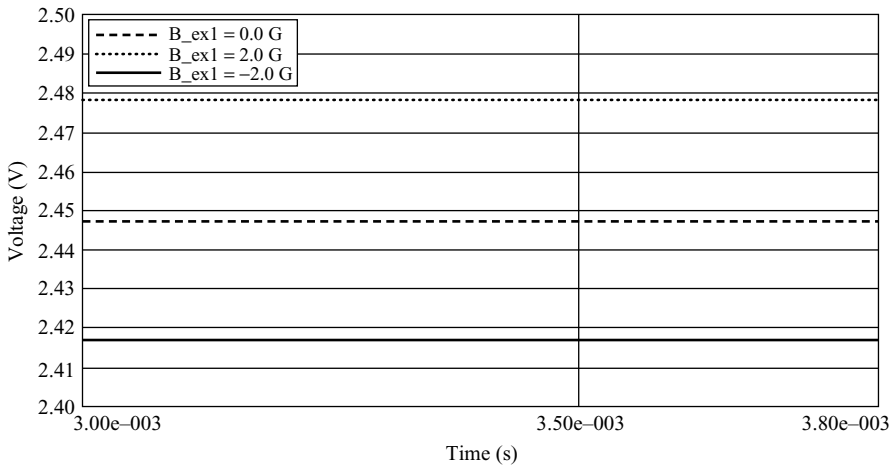

FIGURE 11.19 Computed output voltages of Figure 11.18 model.

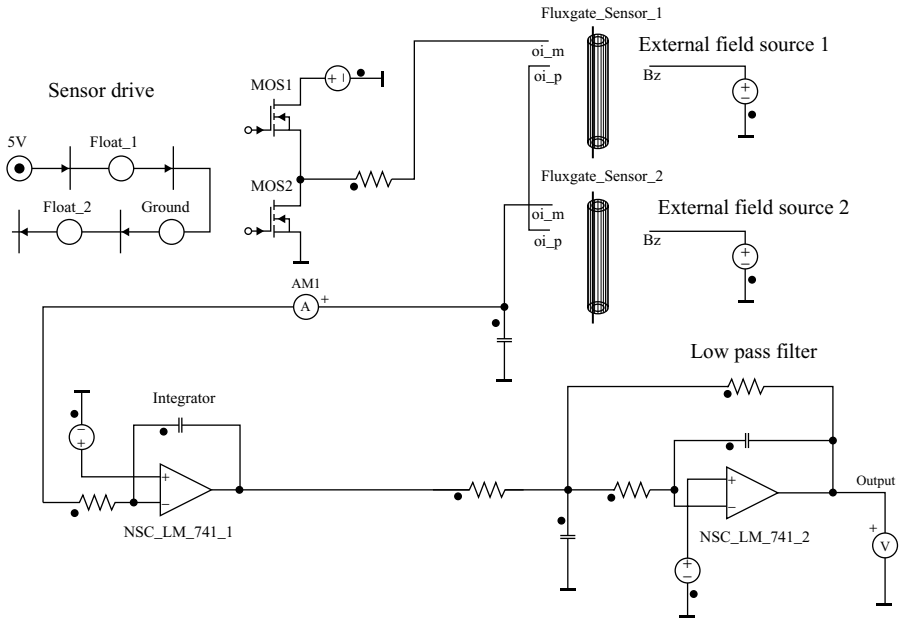

FIGURE 11.20 A systems model of two-field differential fluxgate sensor. The MOSFETs are fired by a state machine model, commonly used in control systems.

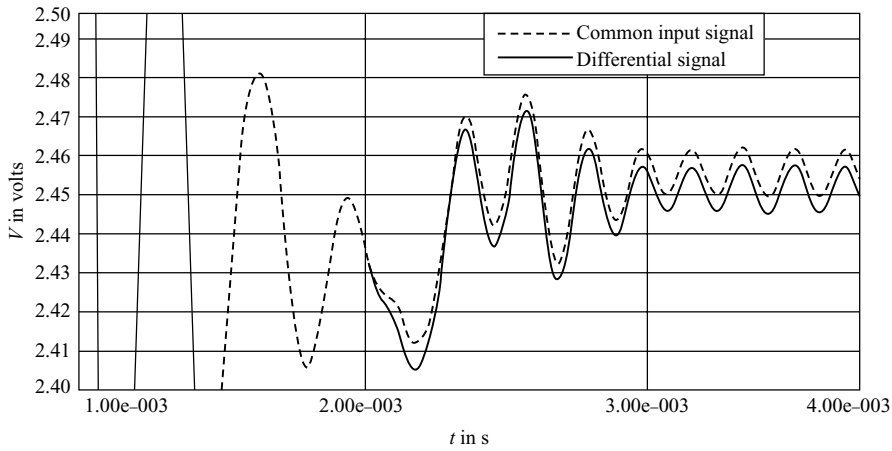

FIGURE 11.21 Computed transient response of sensor of Figure 11.20 to a step change in external field from 0 to −0.2 mT. The common and differential voltages are plotted on the vertical axis, and time in seconds is plotted along the horizontal axis.

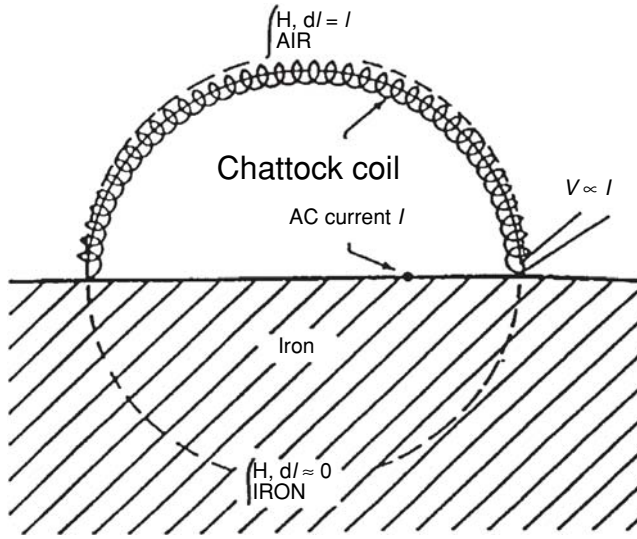

FIGURE 11.22 Chattock coil and its use to determine the line integral of $\mathbf{H}$ = MMF = AC current I enclosed.

core and thus is lightweight, it can be easily moved over iron surfaces to detect AC currents. Both impressed currents and induced eddy currents can be detected using their magnetic fields [17]. Very similar to the Chattock coil is the Rogowski coil, which usually has an arc closer to 360°; both are named after their inventors.

The AC voltage induced in the Chattock coil is derived by applying Faraday's law:

$$V = -N\frac{d\varphi}{dt} \tag{11.11}$$

where N is the number of turns and the magnetic flux φ is sinusoidal with $\varphi = \varphi_{\text{peak}}$ $e^{j\omega t}$. The flux is $\varphi = B\,A$ where B is the flux density and A is the cross-sectional area of the coil. Since the Chattock coil has an air core and μ_o is the permeability of free space, we obtain:

$$V = -jNA\omega\mu_o H \tag{11.12}$$

In Figure 11.22 with one coil at one location:

$$V = -jNA\omega\mu_o H_{\text{ave}} \tag{11.13}$$

which can be rewritten as:

$$V = -jA\omega\mu_o(NH_{\text{ave}}) \tag{11.14}$$

For each turn of the Chattock coil, this becomes:

$$V = -jA\omega\mu_o(L_T N_L H_{\text{ave}}) \tag{11.15}$$

where L_T is the Chattock coil turn length, and N_L is the number of turns per unit length. If the average of the flux intensity over the entire length of the Chattock coil of Figure 11.22 is examined, a final substitution can be made to obtain:

$$V = \mu_o \omega N_L A \int H \cdot dl \tag{11.16}$$

Applying Ampere's circuital law to Figure 11.22 and assuming $\boldsymbol{H} = 0$ in the iron (due to its high permeability), (11.14) becomes:

$$V = \mu_o \omega N_L A I \tag{11.17}$$

Thus the Chattock coil output voltage is directly proportional to the current enclosed I, which in many cases is the eddy current induced in the iron [17]. For example, steel laminations in the stators of large generators may be damaged such that their interlaminar insulation fails and thus contains large eddy currents. The magnetic field produced by the eddy currents is commonly detected and located by scanning with a Chattock coil [17].

11.8 SQUID MAGNETOMETERS

Magnetometer is a term commonly used for very sensitive magnetic field sensors. Fluxgate sensors can be used in magnetometers.

SQUID stands for *s*uperconducting *qu*antum *i*nterference *d*evice, and is the most sensitive way of measuring magnetic fields at frequencies as low as 1 Hz (essentially DC). Unfortunately, the superconducting (zero resistance) coils require cooling to very low temperatures.

If magnetic flux passes through a ring made of a superconducting material as shown in Figure 11.23, a current is induced in the ring. Without any disturbances the

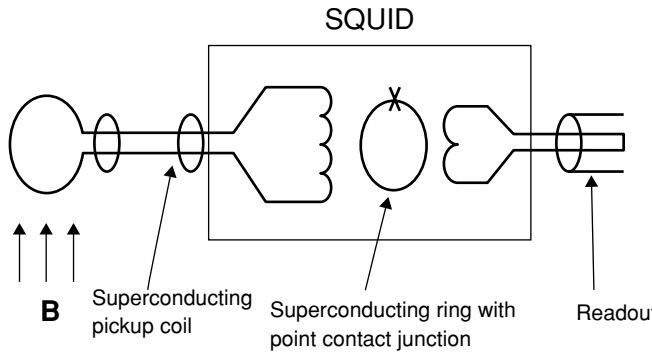

FIGURE 11.23 A schematic of SQUID. The current in the readout coil is proportional to the magnetic flux density being sensed.

current would continue flowing forever. The magnitude of the induced current is an extremely sensitive indicator of the flux density. It turns out that the flux through the ring is quantized in that the flux can only take on values that are integer multiples of a basic flux quantum.

To measure the current in the superconducting ring, a Josephson junction is used. It is a thin layer of insulation or a narrowing of the superconductor to form a weak link. In 1962, Josephson predicted that a supercurrent could flow through this weak link that would be an oscillating function of the magnetic field intensity in the weak link. The periodic variations in this supercurrent produced by the quantized flux can accurately measure the magnetic field to be sensed. The periodic variations in the current have the same pattern as the interference fringes produced by the diffraction of light, and are related to the flux quantization. Usually, the ring is inductively coupled to a radio-frequency circuit that supplies a known bias field and yields the detector output current. Sensitivity is increased by coupling the ring with the weak link to a larger superconducting ring without a weak link, as shown in Figure 11.23 [18].

The sensitivity of SQUIDs is of the order of 10 fT or 1.E−14 T, approximately the most sensitive level in Figure 10.1. The ability to set a null level by adjusting the bias field in the radio-frequency circuit makes the device particularly useful for differential field measurements. For example, if the null level is set to the average flux density of the earth, the SQUID will readily detect anomalies in the field. The sensing loop can be configured to be sensitive to a gradient in the measuring field by cross-connecting two parallel turns. Because the sense loop is superconducting, it has an essentially DC response to magnetic fields. By orienting the coils properly, the gradient of a component of the external field in any direction can be sensed, which is important in magnetic separators as discussed in Chapters 5 and 7. The ability to fabricate a high sensitivity gradiometer that can measure the partial derivatives of (5.26) is a unique advantage of this technology over other magnetic sensors [18].

Quantum mechanics is also involved in Magnetic Resonance Imaging (MRI), which has been analyzed elsewhere [19]. Sometimes, magnetic ferrite nanoparticles are used to provide contrast in MRI, and such particles are also being investigated for DNA testing [20].

11.9 MAGNETOIMPEDANCE AND MINIATURE SENSORS

Some of the newest developments in sensors are for *magnetoimpedance (MI)* sensors. MI sensors were developed in Japan on micromachined chips in 2001 and 2002 [21]. At that time, they were made of amorphous FeCoSiB wire that had been tension-annealed for surface anisotropy. Their impedance changes due to skin effects and is proportional to the square root of the externally applied magnetic field. More recently, other materials have been used and the response has been made linear with the applied field [22–24].

Various magnetic sensor types are compared in Table 11.1. Note that MI sensors make good magnetometers, for their resolution is down to the same nanotesla range as fluxgate sensors. The speeds in Table 11.1 can be considered to be bandwidths;

TABLE 11.1 Comparison of Sensor Types

Type	Length	Sensitivity	Speed	Wattage
Hall	100 μm	0.5 E−4 T	1 MHz	10 mW
MR	100 μm	0.1 E−4 T	1 MHz	10 mW
GMR	100 μm	0.01 E−4 T	1 MHz	10 mW
Fluxgate	20 mm	0.1 E−9 T	5 kHz	1 W
MI	2 mm	0.1 E−9 T	1 MHz	10 mW

all are 1 MHz except for fluxgate sensors. Not in the table is a new type of magnetic sensor called a *magnetic microwire* [25] which uses magnetostriction in a glass-coated permeable wire to remotely detect stresses in materials.

The lengths in the table are minimum dimensions; note that fluxgate sensors require the most space, followed by MI sensors. Fluxgate sensors also require more input power; the other types only require about 10 mW. Miniaturization to sizes well below 1 mm not only reduces size and weight, but also reduces power requirements. Reduced input power for battery-powered sensors enables reduced battery size and may even enable sensors to be powered by new *energy-harvesters*. These devices generate power from motion or vibration of mobile platforms such as automobiles.

The sensors in Table 11.1 with lengths of 100 μm can be used to make *motes*, which are remote wireless sensors. Of very recent development, motes are sometimes called *smart dust*. If inexpensive enough, hundreds or more could be sprinkled around a region to monitor its detailed magnetic field distribution. IEEE standard 802.15.4 has been enhanced to cover wireless mesh networks called "ZigBee." IEEE standard P1451.4 enables *smart sensors* to *plug and play* into computers, including note book and smaller computers. In automobiles, trucks, and construction equipment, sensors are commonly interfaced using CAN BUS standard technology.

11.10 MEMS SENSORS

Microelectromechanical systems (MEMS) include miniature magnetic sensors and actuators. With all dimensions much less than 1 mm, MEMS actuators have limited output force and are therefore of limited use. MEMS magnetic sensors, however, can output useful voltage or current and thus are increasingly being developed. MEMS sensors are usually made by special techniques used in semiconductor chip manufacture, including *micromachining*.

Many MEMS magnetic sensors use Lorentz force. For example, a miniature bar-shaped permanent magnet moves in a magnetic field without requiring input power. The motion can be detected optically or by other means to sense magnetic fields as small as 200 nT [18]. Such MEMS Lorentz force sensors are linear over a huge range to as high as 50 T [26].

Another MEMS sensor is called the xylophone resonator [18]. A MEMS beam is supplied an AC current with frequency equal to its mechanical resonant frequency. A

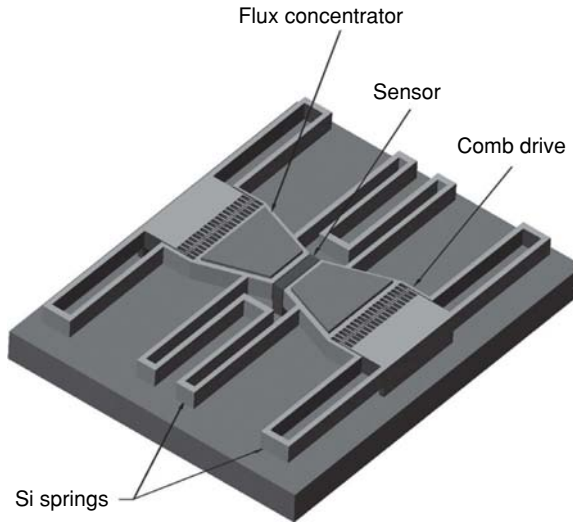

FIGURE 11.24 A MEMS flux concentrator [17]. There is a space between the substrate and the flux concentrators on the MEMS permeable flaps.

DC magnetic field applied perpendicular to the beam axis then vibrate the beam with amplitude proportional to the magnetic field. The vibration amplitude is detected optically.

A MEMS device that concentrates magnetic fields and thus improves the sensitivity of magnetic sensors is the flux concentrator shown in Figure 11.24. It is made of a silicon substrate and soft magnetic flux concentrator flaps. According to the reluctance concepts of Chapter 3, decreasing the gap between the flaps increases the flux density at the sensor. The flaps are forced to oscillate by the applied AC voltage to the two electrostatic comb drives. Typically the MEMS structure resonates mechanically at about 10 kHz, modulating the field at the sensor to increase the operating frequency and the signal-to-noise ratio. Thus the flux concentrators should increase the sensitivity by one to three orders of magnitude [18]. Chapter 13 will further discuss signal-to-noise ratio.

PROBLEMS

11.1 Redo Example 11.1 when the ampere-turns are reduced from 1000 to 500.

11.2 Redo Example 11.2 when the head core relative permeability is reduced to 200.

11.3 Redo Example 11.3 when the frequency is changed to: (a) 100 Hz, (b) 200 Hz, (c) 400 Hz.

11.4 Redo Example 11.3 when the target material is changed to steel with relative permeability 100 and conductivity 1.E6 S/m.

11.5 Find the LVDT output voltage for Example 11.4 when the frequency is increased to 5 kHz.

11.6 Find the LVDT output voltage for Example 11.4 when the armature position is: (a) –4 mm, (b) +2 mm, c) +6 mm.

REFERENCES

1. Jorgensen F. *The Complete Book of Magnetic Recording*, Blue Ridge Summit, PA: TAB Books Inc.; 1980.
2. Comstock RL. *Introduction to Magnetism and Magnetic Recording*, New York: John Wiley & Sons; 1999.
3. Mayergoyz ID. *Mathematical Models of Hysteresis and Their Applications*, 2nd ed. New York: Academic Press; 2003.
4. Della Torre E. *Magnetic Hysteresis*, New York: Wiley-IEEE Press; 2000.
5. VanderHeiden RH, Arkadan AA, Brauer JR. Nonlinear transient finite element modeling of a capacitor discharge magnetizing fixture. *IEEE Trans Magn* 1993; 29: 2051–2054.
6. Kobayashi M, Horowitz R. Track seek control for hard disk dual-stage servo systems. *IEEE Trans Magn* 2001; 37: 949–954.
7. Ashar KG. *Magnetic Disk Drive Technology: Heads, Media, Channel, Interfaces, and Integration*, New York: Wiley-IEEE Press; 1996.
8. Ida N. *Numerical Modeling for Electromagnetic Non-Destructive Evaluation*, London: Chapman & Hall; 1995.
9. Gotoh Y, Takahashi N. Proposal of detecting method of plural cracks and their depth by alternating flux leakage testing: 3D nonlinear eddy current analysis and experiment. *IEEE Trans Magn* 2004; 40: 655–658.
10. Woodson HH, Melcher JR. *Electromechanical Dynamics*, New York: John Wiley & Sons; 1968.
11. Rodger D, Leonard PJ, Karaguler T. An optimal formulation for 3D moving conductor eddy current problems with smooth rotors. *IEEE Trans Magn* 1990; 26: 2370–2372.
12. Ida N, Bastos JPA. *Electromagnetics and Calculation of Fields*, 2nd ed. New York: Springer-Verlag; 1997. pp 420–422.
13. Jay F (ed.). *IEEE Standard Dictionary of Electrical and Electronic Terms*, 2nd ed. New York: Wiley-Interscience; 1977.
14. Chen Y, Snyder JE, Schwichtenberg CR, Dennis KW, McCallum RW, Jiles DC. Metal bonded Co-ferrite composites for magnetostrictive torque sensor applications. *IEEE Trans Magn* 1999; 35: 3652–3654.
15. Steward D. *Fluxgate Sensor Analysis*, Pittsburgh, PA: Power Point presentation prepared for Ansoft Corporation; 2002.
16. Davis ML, Wiegand: the man, the effect, the wire. *Motion Systems Design* 2011; 24–28.
17. Rettler RE, Brauer JR, Ravenstahl M. Finite element eddy current computations in turbo-generator rotors and imperfect stators. *IEEE Int Electric Machines & Drives Conf* 2005; 1598–1605.
18. Lenz J, Edelstein AS. Magnetic sensors and their applications. *IEEE Sensors J* 2006; 6: 631–649.

19. Jin J. *Electromagnetic Analysis and Design in Magnetic Resonance Imaging*, Boca Raton, FL: CRC Press; 1998.
20. Hoffman A. Magnetic viruses for biological and medical applications. *Magnetics Business & Technology* 2005; 24: 1–3.
21. Mohri K, Uchiyama T, Shen LP, Cai CM, Honkura Y, Aoyama H. Amorphous wire and CMOS IC-based sensitive micromagnetic sensors utilizing magnetoimpedance (MI) and stress-impedance (SI) effects. *IEEE Trans Magn* 2002; 38: 3063–3068.
22. Delooze P, Panina L, Mapps D, Ueno K, Sano, H. Sub-nano tesla resolution differential magnetic field sensor utilizing axymmetrical magnetoimpedance in multilayer films. *IEEE Trans Magn* 2004; 40: 2664–2666.
23. Sandacci S, Makhnovskiy D, Panina L, Mohri K, Honkura Y. Off-diagonal impedance in amorphous wires and its application to linear magnetic sensors. *IEEE Trans Magn* 2004; 40: 3505–3511.
24. Wang X, Yuan W, Zhao Z, Li X, Ruan J, Yang X. Giant magnetoimpedance effect in CuBe/NiFeB and CuBe/Insulator/NiFeB electroless-deposited composite wires. *IEEE Trans Magn* 2005; 41: 113–115.
25. Praslička D, Blazek J, Smelko M, Hudak J, Cverha A, Mikita I, Varga R, Zhukov A. Possibilities of measuring stress and health monitoring in materials using contactless sensor based on magnetic microwires. *IEEE Trans Magn* 2013; 49: 128–131.
26. Ripka P, Janosek M. Advances in magnetic field sensors. *IEEE Sensors J* 2010; 10: 1108–1116.